Biomaterials Science

PAPER

View Article Online
View Journal | View Issue

Cite this: *Biomater. Sci.*, 2017, **5**, 1293

Diabetic wound regeneration using heparin-mimetic peptide amphiphile gel in db/db mice†

Berna Senturk,[a] Burak M. Demircan,[b] Alper D. Ozkan,[a] Sehmus Tohumeken,[a] Tuncay Delibasi,*[c,d] Mustafa O. Guler*[a,e] and Ayse B. Tekinay*[a,b]

Received 25th March 2017,
Accepted 11th May 2017

DOI: 10.1039/c7bm00251c

rsc.li/biomaterials-science

There is an urgent need for more efficient treatment of chronic wounds in diabetic patients especially with a high risk of leg amputation. Biomaterials capable of presenting extracellular matrix-mimetic signals may assist in the recovery of diabetic wounds by creating a more conducive environment for blood vessel formation and modulating the immune system. In a previous study, we showed that glycosaminoglycan-mimetic peptide nanofibers are able to increase the rate of closure in STZ-induced diabetic rats by induction of angiogenesis. The present study investigates the effect of a heparin-mimetic peptide amphiphile (PA) nanofiber gel on full-thickness excisional wounds in a db/db diabetic mouse model, with emphasis on the ability of the PA nanofiber network to regulate angiogenesis and the expression of pro-inflammatory cytokines. Here, we showed that the heparin-mimetic PA gel can support tissue neovascularization, enhance the deposition of collagen and expression of alpha-smooth muscle actin (α-SMA), and eliminate the sustained presence of interleukin-6 (IL-6) and tumor necrosis factor-alpha (TNF-α) in the diabetic wound site. As the absence of neovascularization and overexpression of pro-inflammatory markers are a hallmark of diabetes and interfere with wound recovery by preventing the healing process, the heparin-mimetic PA treatment is a promising candidate for acceleration of diabetic wound healing by modulating angiogenesis and local immune response.

1. Introduction

Diabetes mellitus is a multi-systemic chronic disease that is associated with severe wound infections. Type 2 diabetes mellitus is the most common type of diabetes in humans and presents as hyperglycemia resulting from a combination of insulin resistance and reduction in insulin secretion in later stages.[1] Both type 1 and type 2 diabetic patients suffer from delayed wound healing and the potential progression of skin wounds into diabetic ulcers, which affect roughly 5% of diabetic patients and remains a major concern for diabetes management.[2] Biomaterials capable of enhancing the repair of diabetic wounds are, therefore, promising for improving the quality-of-life of diabetic patients.[3]

Diabetic wounds are characterized by the low expression of angiogenic growth factors, prolonged inflammation, impaired cellular activity and relative lack of skin tissue remodeling.[4,5] During wound healing, growth factors are released from a broad variety of cells and provide the signals required for wound closure. The reduced expression of angiogenic growth factors, such as vascular endothelial growth factor (VEGF), is strongly associated with the failure of angiogenesis.[6] Angiogenesis is a critical aspect of wound healing since it primarily facilitates the transfer of oxygen and nutrients to the wound site during the proliferative and remodeling phases of wound healing. The inhibition of angiogenesis therefore imposes severe constraints to the metabolic resources that are available at the site of injury, and may consequently prevent wound closure in diabetic patients. Wound closure is further delayed in diabetic mice due to the sustained expression of pro-inflammatory cytokines such as interleukin 6 (IL-6) and tumor necrosis factor-alpha (TNF-α) at the wound site.[7] Non-healing wounds are also characterized by the overexpression of IL-6 and associated with skin pathologies such as psoriasis, while chronic increments in the expression of TNF-α is associated with decreased collagen deposition and impaired wound healing.[8–10] On the other hand, IL-6 deficient (IL-6 KO) mice

[a]*Institute of Materials Science and Nanotechnology, National Nanotechnology Research Center (UNAM), Bilkent University, Ankara, 06800, Turkey. E-mail: mguler@uchicago.edu, atekinay@bilkent.edu.tr*
[b]*Neuroscience Graduate Program, Bilkent University, Ankara, 06800, Turkey*
[c]*ADACELL Cell Therapy, Regenerative Medicine and Research Hospital Etlik Polyclinic, Department of Endocrinology and Metabolism, Ankara, 06010, Turkey. E-mail: tuncay@delibasi.net*
[d]*Department of Internal Medicine, School of Medicine (Kastamonu), Hacettepe University, Ankara, 06100, Turkey*
[e]*Institute for Molecular Engineering, University of Chicago, Chicago, IL 60637, USA*
†Electronic supplementary information (ESI) available. See DOI: 10.1039/c7bm00251c

show severe impairments in wound healing compared to wild type control animals, suggesting that inflammatory cytokines also play a fundamental role in initiating the healing response.

Diabetic animal models are produced either by chemical induction (most commonly with STZ) or through systemic mutations such as obese/obese (ob/ob) and diabetes/diabetes (db/db mice).[11] Although chemically induced diabetes provides a simple and relatively cheap diabetic model, there is some evidence that it is not completely representative of diabetes in humans.[12] On the other hand, genetic models allow the investigation of the natural mechanisms of diabetes without the potential side effects associated with chemical treatment, and obese models (ob/ob, db/db) of type 2 diabetes are especially close to the human disease, as these animals naturally develop hyperglycaemia as a consequence of obesity and exhibit many of the symptoms observed in type 2 diabetic patients. In particular, the db/db mouse model is among the most popular models of diabetes, and also causes obesity at the age of 4 weeks. These mice become hyperinsulinemic at around the age of 2 weeks and develop a resistance to insulin, eventually (4–8 weeks) exhibiting advanced hyperglycaemia due to beta cell failure.[13] While diabetes is also very severe in ob/ob mice, the underlying cause of diabetes in this strain is a deficiency in leptin rather than leptin receptors, and ob/ob mice do not exhibit complete beta cell failure. As such, ob/ob mice are generally not considered to be representative of human diabetes.[11] Therefore, the db/db mouse model was chosen to accurately reflect the pathophysiology of diabetes and investigate whether heparin-mimetic PA treatment is able to reduce the abnormalities in wound healing normally seen in diabetic injuries.

Peptide amphiphile molecules have received considerable attention in the recent decades due to their ability to present bioactive signals without necessitating the production and isolation of complex proteins from xenogenic sources. In addition, the nanofibrous networks formed by PA assemblies closely resemble the structure of the extracellular matrix and allow PA molecules to effectively present their bioactive epitopes to their target cells. We had previously developed a PA-based material that is able to enhance angiogenesis both *in vitro* and *in vivo* by mimicking the inductive signals inherent to heparin molecules.[14] The bioactive PA nanofibers in particular exhibit a strong potential to accelerate the wound healing process by protecting and improving the bioavailability of various growth factors.[15] Heparin PA treatment improved wound healing in STZ-induced diabetic rats by induction of neovascularization.[16] In the current study, wound healing capacity of a heparin-mimetic gel was analyzed in the db/db diabetic wound model. Although modulation of monocyte/macrophage number upon treatment was investigated in STZ-induced rats, the effect of PA treatment on the inflammatory phase was not clear.[16] In this study, the anti-inflammatory effect of the heparin mimetic gel was analyzed for the first time by pro-inflammatory markers IL-6 and TNF-α.

Here, we demonstrate the effect of heparin-mimetic PA nanofiber gels on the recovery of diabetic wounds by analyzing the wound healing rate, re-epithelialization, granulation tissue formation, blood vessel density and the inflammatory response of full skin thickness wounds in db/db transgenic mice. In addition, the effect of heparin-mimetic nanofibers on the expression of VEGF and the pro-inflammatory cytokines IL-6 and TNF-α was examined. The progression of wound healing was compared between the bioactive gel treated and PBS control diabetic mice. The efficacy of heparin-mimetic gel treatment was evaluated and we show potential usage of the heparin-mimetic gel on healing of chronic wounds.

2. Materials and methods

2.1. Materials

6 mm biopsy punches were purchased from Microtek Medical, Zutphen NL. ELISA antibodies for IL-6 (14-7061) and TNF-α (CMC3013) were purchased from eBioscience and Life Technologies, respectively. Db/db transgenic mice were supplied from Indiana, USA. All ELISA reagents were purchased from Life Technologies. For peptide synthesis, 9-fluorenylmethoxycarbonyl (Fmoc) and *tert*-butoxycarbonyl (Boc) protected amino acids (except glyco-amino acid), [4-[α-(2′,4′-dimethoxyphenyl)fmocaminomethyl]phenoxy]acetamidonorleucyl-MBHA resin (Rink amide MBHA resin) and 2-(1*H*-benzotriazol-1-yl)-1,1,3,3-tetramethyluronium hexafluorophosphate (HBTU) were purchased from NovaBiochem. Methylene chloride (DCM), *N*,*N*-dimethylformamide (DMF) and trifluoroacetic acid (TFA) solutions were purchased from Sigma Aldrich.

2.2. Peptide synthesis and self-assembled nanofibrous network formation

Functionalized PA molecules were synthesized by standard solid phase Fmoc peptide synthesis chemistry. For heparin-mimetic PA synthesis, Lauryl-VVAGEGDK(pbs)S-Am (GAG-PA) and Lauryl-VVAGK-Am (K-PA) were synthesized on Rink amide resin. Amino acid coupling reactions were performed with 2 equivalents of Fmoc-protected amino acid, 1.95 equivalents of HBTU, and 3 equivalents of DIEA for 4 h. The Fmoc protecting group was removed with 20% piperidine/DMF solution for 20 min. Peptides were cleaved from the resin using 95 : 2.5 : 2.5 TFA/TIS/H_2O for 3 h. Excess TFA was removed by rotary evaporation. The remaining peptide was precipitated with ice-cold diethyl ether and freeze-dried. The peptide was characterized by quadruple-time-of-flight mass spectrometry (Q-TOF MS) and purified with reverse phase preparative HPLC (Fig. S1†).

Nanofibers were formed by mixing negatively charged GAG-PA and positively charged K-PA at pH 7.4 at a 1 : 2 ratio, respectively. The net charge of the system is −1. It was previously shown that the negative charge of the peptide is critical for the binding capacity of the heparin-mimetic nanofiber to VEGF.[14,15] Aqueous solutions of peptide amphiphiles were prepared in double distilled water.

2.3. Transmission electron microscopy (TEM)

GAG-PA/K-PA peptide nanofibers were diluted from 10 mM stock to 50 μM for TEM sample preparation. Peptide nano-

fibers were placed on a TEM grid, incubated for 7 min and stained with 2 wt% uranyl-acetate for 1 min. Imaging was performed with a FEI Tecnai G2 F30 TEM at 200 kV.

2.4. Scanning electron microscopy (SEM)

A mixture of GAG-PA and E-PA was prepared on a silicon wafer and incubated for 20 min for gelation. Peptide samples were dehydrated through gradually increasing the concentrations of ethanol solutions and completely dried in a critical point dryer. The samples were coated with a 5 nm-thick Au–Pd layer and imaged by using a FEI Quanta 200 FEG SEM, using the GSED detector at an ESEM mode with 3–10 keV beam energy.

2.5. Circular dichroism analysis

Secondary structures of nanofibers were assessed by circular dichroism (CD) analysis using a J-815 Jasco spectrophotometer. 3.6×10^{-4} M aqueous solutions of peptide amphiphiles were used for CD spectroscopy. Measurements were acquired at room temperature with a 500 nm min^{-1} scanning speed, 1 nm bandwidth and 0.1 nm data pitch within the data interval of 300 to 190 nm. Measurements were repeated three times and averaged for each sample. The results were represented as molar ellipticity.

2.6. Oscillatory rheology

Oscillatory rheology measurements were performed with an Anton Paar Physica MCR301. 10 mM of GAG-PA and K-PA were mixed in a 1 : 2 ratio as used in experiments. Rheological analyses were performed, angular frequency was kept constant at 10 rad s^{-1}, and strain was increased between 0.1 and 100%. Storage and loss moduli were recorded accordingly.

2.7. Animals and wound healing model

All animal experiments were performed on 12–16 week old, genetically diabetic mice (db/db; BKS.Cg-+$Lepr^{db}$/+$Lepr^{db}$/OlaHsd, USA, IN) in accordance with the guidelines set by the Diskapi Hospital Animal Ethics Committee after obtaining their official approval.

Mice were anesthetized with xylazine hydrochloride (Alfazyne, 10 mg kg^{-1}) and ketamine hydrochloride (Alfamine, 25 mg kg^{-1}) and randomly divided into two cohorts as control (n = 6) and GAG-PA/K-PA treated (n = 6) groups. Two full-thickness circular wounds with 6 mm diameters were created on each animal using disposable biopsy punches. One wound was treated with GAG-PA/K-PA while the other one was treated with PBS on the same animal (Fig. 2B). There is no side preference for the treatment, the right side of the equal number of animals was treated with GAG-PA/K-PA or PBS solution. All wounded mice were housed individually. The wounding operation and postoperative treatments were performed by the same researcher. Bioactive gels were applied topically to the wound area at a volume of 300 μL and a concentration of 1% (w/v). Similarly, control wounds were treated with 300 μL of PBS solution. Both treatments were applied for 2 days. All wounds were covered with Octacare non-woven wound dressing (OCTAMED) to prevent the leakage of materials from the wound site. Animals were sacrificed on days 7, 14 and 21 for analysis.

2.8. Wound analysis

Mice were anesthetized with xylazine hydrochloride and ketamine hydrochloride prior to wound closure measurements. The wounds were photographed (days 7, 14, 21) and replicated on transparent tracing paper (by tracing the border of the wound covered with epithelium) to calculate the percentage of wound closure. The paper was then scanned and transferred into cross-sectional paper, and wound sizes were analyzed using ImageJ software.

2.9. Histological analysis

Removed skin tissues were fixed in 10% formaldehyde for 24 h, embedded in paraffin and sectioned in 5 μm increments. Hematoxylin–eosin (H&E) staining was performed for the determination of the wound healing progress in the wound bed, and Masson's trichrome staining was performed for collagen deposition and granulation tissue analysis. Prior to both stainings, paraffin was removed with xylene washing and tissue sections were rehydrated through graded alcohols to distilled water. Rehydrated samples were either stained with H&E or immersed in phosphomolybdic acid, aniline blue, acetic acid and ethanol for Masson's trichrome staining. H&E- and Masson's trichrome-stained tissue sections were visualized on an up-right microscope (Zeiss Axio Scope A1).

The collagen content and organization were further investigated with Picrosirius red. Picrosirius staining was performed with a counterstaining of hematoxylin. Slides were incubated in 0.1% Sirius red in saturated picric acid for 1 hour at room temperature. They were then washed with acidified water, dehydrated through ethanol and xylene, and sealed with mounting medium. Picrosirius red staining slides were imaged under polarized-light microscopy (Zeiss Axio Imager.A2 m).

For quantification of percentage of granulation tissue per total wound area, H&E stained tissue sections from each wound were used. The whole granulation tissue area was traced, measured with ImageJ and divided the total wound area. To determine the percentage of re-epithelialization, the length of the newly formed epithelium and the distance between the original wound margins were measured using the ImageJ software and following formula was used:

$$\%\,\text{re-epithelialization} = [\text{length of new epithelium}]/[\text{distance between the original wound margins}] \times 100$$

Measurement procedures were performed by two researchers blind to the study group.

2.10. Immunohistochemistry

Tissue sections were deparaffinized by heat, immersed in xylene, rehydrated, and washed in distilled water. For antigen retrieval, samples were treated with citrate buffer in a steamer at 100 °C for 10–15 min. Endogenous peroxidase activity was blocked by placing the sections in 3% hydrogen peroxide for

10 min. Non-specific staining was blocked with normal goat serum, and the sections were incubated overnight with the monoclonal von Willebrand Factor antibody (rabbit, ab6994, Abcam, 1 : 500) at 4 °C. After washing, a horse radish peroxidase (HRP)-labeled secondary antibody (anti-rabbit, ab6721, Abcam, 1 : 500) was applied for 1 h at room temperature, and the samples were then treated with diaminobenzidine (DAB).

The number of blood vessels was counted from the wound area with positive staining of von Willebrand Factor staining for each section and quantified by two independent observers. The ImageJ analysis system was used to calculate the number of vessels in each field.

2.11. Protein isolation and western blotting

Skin samples were homogenized in the Trizol® reagent, and the protein-containing supernatant was removed and stored at −80 °C. Protein concentrations were determined using the BCA Protein Assay Kit. Equal amounts of proteins per lane (50 μg) were separated by 5–12% SDS-PAGE and transferred to a polyvinylidene difluoride (PVDF) membrane. The membrane was blocked with 5% non-fat milk in TBS-T at room temperature for 2 h and then incubated overnight with an anti-VEGF antibody (ABS82, Millipore, 1 : 2000) or α-SMA antibody (Millipore, 1 : 50 000) at 4 °C. After washing in TBS-T, the blots were incubated with a HRP-coupled secondary antibody (12–349, Millipore, goat anti-rabbit IgG; 1 : 2000). The bands were visualized using the Clarity™ western ECL blotting substrate. GAPDH (Millipore; 1 : 1000) was used as the internal control and treated with the same protocol. Protein amounts in each sample were quantified using ImageJ software.

2.12. ELISA

Pro-inflammatory cytokine concentrations in wound tissues were measured at the end of the experiment by sandwich-ELISA. Protein concentrations were determined using the BCA Protein Assay Kit and 50 ng protein samples were used. MaxiSorp™ plates (Thermo Scientific, NUNC) were coated with IL-6 (1 : 1000) (14-7061-81) or TNF-α (1 : 500) (CMC3013) primary antibodies through overnight incubation at 4 °C. On the next day, plates were washed, dried by tapping, blocked with 0.5% BSA (2 h) and incubated with isolated protein from tissues (overnight incubation at 4 °C). On the following day, the protein samples were consecutively labeled with a biotin-labeled secondary antibody (2 h) and HRP-conjugated streptavidin (1 h) at room temperature.

For the determination of both types of collagen (collagen I and collagen III) concentrations, indirect-ELISA was performed. Plates were coated with isolated protein from wound tissues (overnight incubation at 4 °C). On the next day, plates were washed, dried by tapping, blocked with 0.5% BSA (2 h) and anti-collagen III (1 : 500) (ab7778) or anti-collagen I (1 : 500) (ab6308) primary antibodies through overnight incubation at 4 °C. Then, plates were washed 5 times with washing buffer and dried by tapping between each consecutive step. The HRP-conjugated anti-IgG antibody was used as a secondary antibody and incubated for 2 h. The TMB (3,3′,5,5′-tetramethylbenzidine) substrate was added at the last step and the reaction was stopped after 30 min with 1.8 N H_2SO_4. Color formation was measured by using a microplate reader (Spectramax M5, Microplate reader) as absorbance at 450 nm wavelength. In order to obtain exact absorbance values that are attributable solely to dye color, the measured values were subtracted from a reference value (at 650 nm). All treatments were performed with at least three replicates and shown as mean ± standard error of mean.

2.13. Statistical analysis

Statistical analyses were performed using GraphPad Prism 5. Data analysis was carried out using two tailed Student's *t* test with the raw data. Error bars indicate ± SEM (standard error of mean).

3. Results and discussion

3.1. Characterization of self-assembled heparin-mimetic peptide nanofibers

Heparin-mimetic peptide components; Lauryl-VVAGEGDK (pbs)S-Am (GAG-PA) and Lauryl-VVAGK-Am (K-PA) molecules were synthesized by Fmoc solid-phase peptide synthesis. As shown in the chemical structure of peptide amphiphile molecules, they carry a hydrophobic alkyl tail, β-sheet forming sequences and a bioactive epitope group (Fig. 1A). The GAG-PA molecule bears a strong negative charge (−3) due to its glutamate, aspartate and *p*-sulfobenzoic acid-modified lysine residues. On the other hand, K-PA carries a positive charge of +1, which is localized on the protonated amino group of the lysine residue and allows the molecule to serve as a charge-screening entity for the self-assembly of GAG-PA/K-PA.

GAG-PA/K-PA scaffolds were characterized with SEM, TEM and CD analysis. Circular dichroism (CD) spectroscopy analysis of PAs showed that co-assembled systems were oriented in a β-sheet conformation, presenting a negative peak signal at 220 nm and a positive peak signal at 202 nm (Fig. S2A†). While the GAG-PA/K-PA mixture had a β-sheet structure, the individual peptides exhibit a combination of weak β-sheets and random coils due to charge repulsion between the individual peptide units. Structural properties of the PA nanofiber system were further characterized by SEM (Fig. 1C) and TEM imaging (Fig. 1D). The three-dimensional nanofibrous structure of PA nanofibers was found to be quite similar to the natural ECM.[17]

Physical characteristics of the PA assembly matrix are critical for the material to remain at the wound site throughout the recovery period and support cell growth while allowing for cellular migration and recruitment. Mechanical properties of the matrix were investigated with oscillatory rheology. Storage (G') and loss (G'') moduli were scanned from 100 to 0.1 rad s^{-1} of angular frequency and with a constant shear strain. The GAG-PA/K-PA mixture was found to have a higher storage modulus (G') than loss modulus (G''), suggesting that the peptide nanofibers form hydrogels at pH 7.4 (Fig. S2B†).

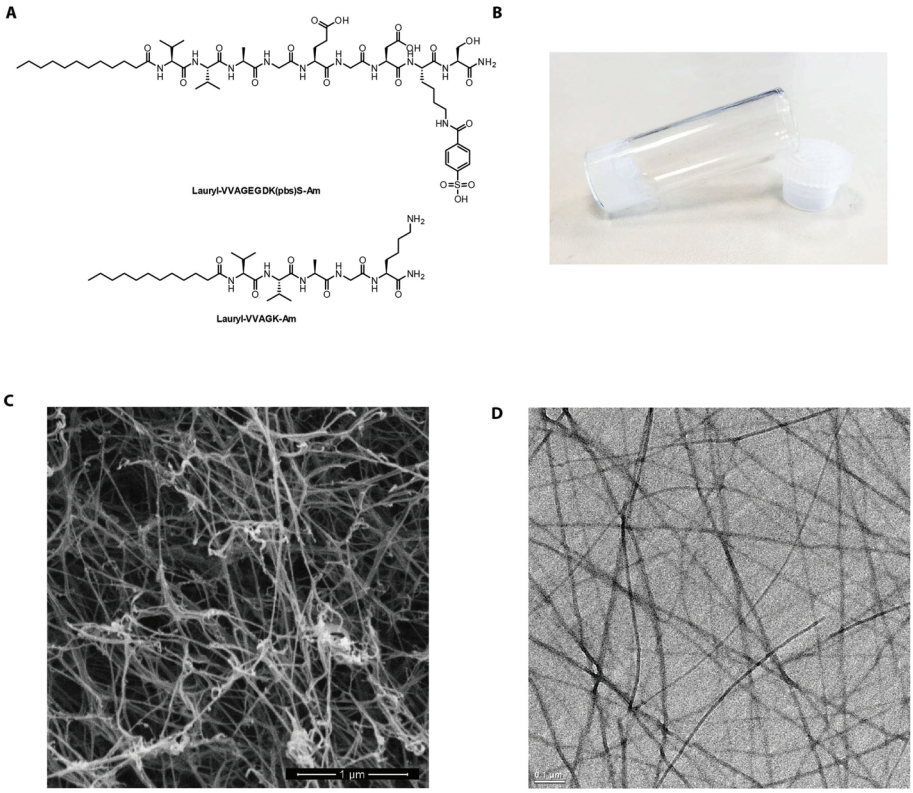

Fig. 1 Chemical view and structural characterization of GAG-PA/K-PA. PAs have three regions; hydrophobic tail (lauric acid), β-sheet forming amino acids (VVAG) and peptide epitopes, as seen in the chemical view (A). Mixing of positively and negatively charged PAs resulted in the formation of gels at pH 7.4 (B). SEM (C) and TEM (D) images of GAG-PA/K-PA show peptide nanofiber networks. Scale bars are 1 μm in SEM and 0.1 μm in TEM images.

Storage modulus results show that the stiffness of the gels was around 7.5 kPa. The viscoelastic behaviors observed in PA scaffolds are favorable, as they are similar to ECM remodeling.[18]

3.2. GAG-PA/K-PA treatment accelerates wound closure

To evaluate the effect of heparin-mimetic peptide treatment on the wound healing process, we first focus on wound closure in db/db mice. The rate of wound closure was only compared between the bioactive gel and PBS control treatment groups; non-bioactive peptide gel control was not used in this study since it did not show any effect on wound healing in the previous study.[16] It has been previously shown that non-bioactive control of GAG-PA/K-PA did not induce angiogenesis either *in vitro* or *in vivo*.[14,15] Since it did not show any positive effect on the wound healing mechanism, the non-bioactive control gel group was not used in this study in order to not increase the number of animals. Two wounds of full-thickness on the dorsal part of the animal were created by using 6 mm diameter biopsy punches and one side was treated with GAG-PA/K-PA and the other side was treated with PBS (Fig. 2B). We analyzed the healing progress of diabetic wounds at different time points throughout 21 days of GAG-PA/K-PA (bioactive gel) and PBS treatment groups. Db/db mice from each group were sacrificed on days 7, 14 and 21 post-treatment for clinical observation, histological and molecular analysis. Fig. 2A shows sequential photographs of two treatment groups on days 7, 14 and 21, respectively. Representative pictures of wounds from diabetic animals indicated that control animals carry scabs even after 21 days of recovery, while bioactive gel treated animals exhibited completely re-epithelialized wounds on day 21 (Fig. 2A). Wound area quantifications showed that GAG-PA/K-PA treated mice showed significantly smaller wounds compared to the PBS control group on days 7, 14 and 21 (Fig. 2C). The wound size was around 44.1% on day 21 in the bioactive gel treated group, while it was 58.4% in the control group. As such, the wound closure was not complete after 21 days even for the GAG-PA/K-PA treated group, but the wound sizes were significantly smaller than the control group.

H&E staining was performed on mouse skin sections to further investigate the changes that occur during the re-epithelialization, granulation tissue formation and tissue remodeling phases (Fig. 3 and 4). Morphological changes on diabetic wounds, such as crust formation (Cr), replacement of the wound matrix (M) and granulation tissue (G) formation were observed on days 7 and 14 in both groups (Fig. 3A). H&E stained sections were analyzed to quantify granulation tissue formation and re-epithelialization in a blinded manner. Histological analysis of healing wounds in db/db diabetic mice showed faster re-epithelialization following GAG-PA/K-PA treat-

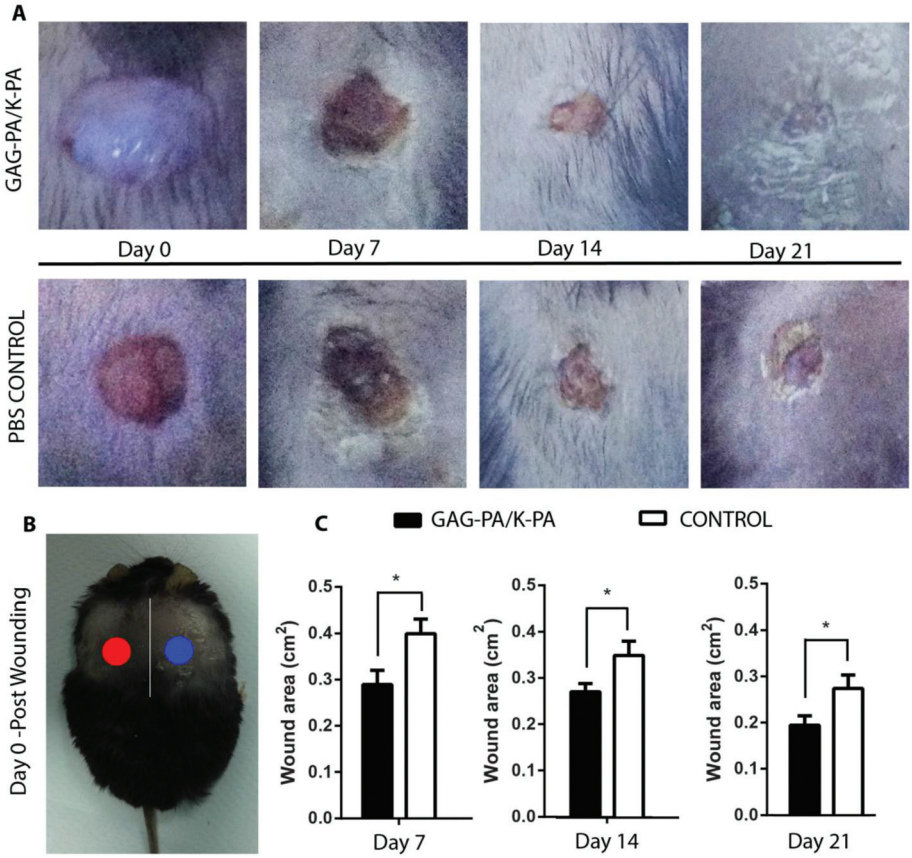

Fig. 2 Bioactive heparin-mimetic peptide nanofiber treatment accelerates the recovery of diabetic wounds. Representative pictures illustrate the closure of wounds in GAG-PA/K-PA and PBS treated animals on days 0, 7, 14 and 21 (A). Two wounds (red and blue circle) were created by biopsy punches at the dorsal skin of db/db mice on day 0 (B). Wound area measurement showed that skin wounds of animals treated with GAG-PA/K-PA nanofibers close faster than control animals, exhibiting smaller average wound areas at days 7, 14 and 21 (C). Values are expressed as mean ± SEM, (n = 6), *p < 0.05.

ment compared to control on day 7 (Fig. 3). Calculation of granulation area per total wound area indicated that the formation of granulation tissue is faster in the bioactive gel treated group on day 7; however, granulation tissue formation rates were similar in later days of wound healing (Fig. 3B) (days 14 and 21). After twenty-one days of recovery, almost the entire wound area was covered by granulation tissue, suggesting that granulation had been successfully completed in both groups (Fig. 3A and B).

Re-epithelialization, which is one of the main markers of successful wound closure, was determined by the measurement obtained from the histological analysis of epithelial tissue. We demonstrated that percentage re-epithelialization was markedly higher in bioactive gel (24.44%) treated mice compared to control (15.25%) on day 7 (Fig. 3C). This result further confirms that bioactive gel treatment promoted wound healing by accelerating wound closure in the early phase of re-epithelialization.

3.3. Collagen determination in wound area

The synthesis and deposition of collagen is essential for the healthy wound healing process. At the beginning of the proliferation phase, the collagen layer in the wound area mainly includes two types of collagens; type I and type III. However, collagen deposition–replacement of type III collagen with type I occurs throughout the wound healing process, and newly deposited collagen is re-aligned at the remodeling phase in particular. Collagen alignment is not only critical for wound contraction, but also determines the severity of scar tissue formation.[19] Therefore, cross-sections of skin tissue were analyzed by Picrosirius red and Masson's trichrome staining, and ELISA to understand whether bioactive gel treatment promotes collagen deposition.

The content and organization of collagens were examined under polarized light with Picrosirius red staining (Fig. 4). In this staining, because of the difference in their pattern of physical aggregation and thickness of collagen fibers the green color represents type III collagen, whereas red color is an indicator of type I collagen.[20] As the wound healing proceeds, the green color denotes thin fibers disappeared and replaced with tightly packed red bundles of type I collagen.[21] As seen in Fig. 4, in the early stage of wound healing (on day 7) green color and red color were present in the wound area (A, C), however red color became more

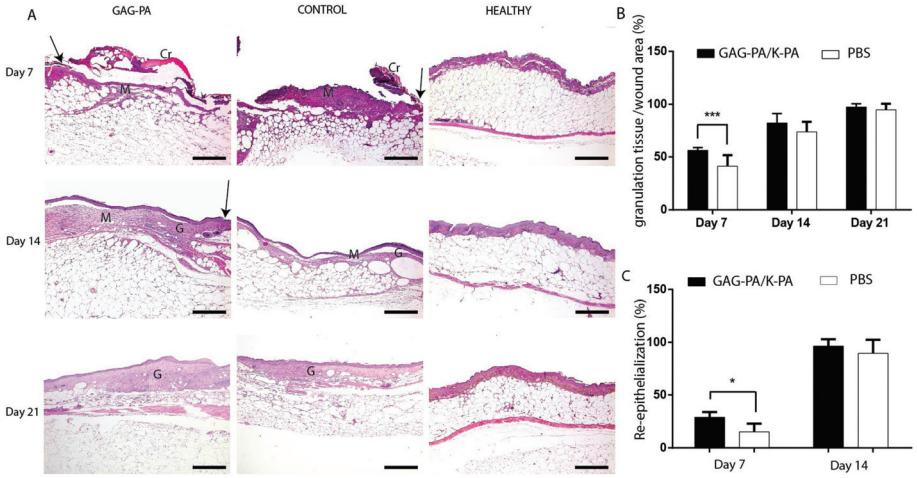

Fig. 3 Histological analysis of H&E stained tissue sections from db/db mice treated with GAG-PA/K-PA and PBS, and unwounded healthy controls. Changes in tissue morphology, such as the formation of a wound crust (Cr), wound matrix (M) and granulation tissue (G) were investigated throughout the recovery period (A). The rate of granulation tissue formation was evaluated by calculating the ratio of the granulation tissue compared to the total wound area (B). In GAG-/PA-K-PA treated mice, re-epithelialization was faster on day 7 compared to PBS control (C). Arrows indicate original wound edge (A). Images were taken with 5× magnification by using an up-right microscope. Values are expressed as mean ± SEM, (n = 6), *p < 0.05, scale bars = 500 μm.

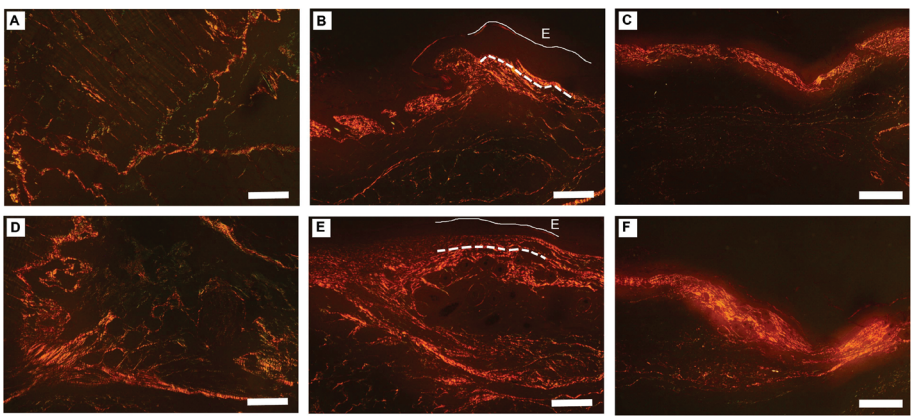

Fig. 4 The content and orientation of collagens in full-thickness diabetic wound samples treated with GAG-PA/K-PA (A–C) and PBS (D–F). Tissue sections were stained with Picrosirius red in picric acid and photographed under cross-polarized light. Images were taken on day 7 (A, D), day 14 (B, E) and day 21 (C, F). Dashed white lines represent orientation of collagens and continuous white lines track border of epidermis (E) on day 14 (B, E). Original magnification is 100× and scale bars are 200 μm.

dominant on day 14 (B, D) in both groups. The alignment of collagen fibers was mostly parallel to the epidermis (continuous white line) in the upper layer (dashed white lines), and reticulated in the dermis and hypodermis on day 14 (Fig. 4B and D). No difference was observed between the bioactive gel and control groups in the sense of collagen organization.

The collagen deposition was further assessed through Masson's trichrome staining, showing that the thickness of the fibers increased with the proximity to the wound edge on day 7 (Fig. 5A). The synthesis of type III collagen reaches maxima around day 7 and then undergoes degradation by matrix metalloproteinases (MMPs).[22] As tissue matured, the replacement of collagen type III (light blue) by collagen type I (dark blue) was detected by Masson's trichrome staining (Fig. S3†). Furthermore, syntheses of type I and III collagens were investigated with ELISA (Fig. 5B) to determine the quality of the ECM deposition. Although the collagen I/III ratio showed no significant differences on day 7, it was significantly higher on day 14 after wounding in GAG-PA/K-PA treated mice compared to control. Both Masson's trichrome staining and ELISA results revealed that the collagen type I/III ratio increased over time in both groups. The type I and III collagen ratio in normal skin is approximately 4 : 1.[23] The collagen type I/III ratio was higher and more closer to normal skin in the bioactive treated group.

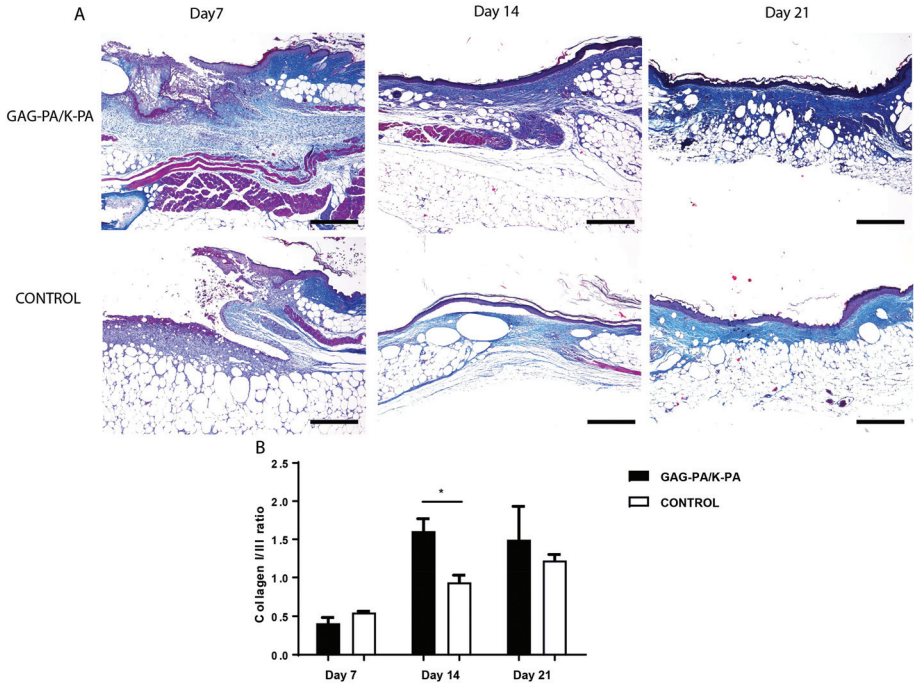

Fig. 5 Masson's trichrome staining of wounds (A) and quantification of the collagen I/III ratio in both groups (B). The staining indicates that granulation tissue formation, re-epithelialization and cell infiltration occur in both groups, but are faster in the bioactive gel treated group on day 14. Data are presented as means ± SEM, $*p < 0.05$, scale bars = 500 μm.

3.4. Angiogenic response was accelerated with increased number of vessels and VEGF expression in heparin-mimetic gel-treated animals

A proper diabetic wound healing requires an angiogenic response which leads to an increase in the number of blood vessels and expression of VEGF at the site of injury.[6] It has been previously shown that heparin-mimetic PA nanofibers trigger the induction of angiogenesis in the cornea and show high binding affinity against $VEGF_{165}$.[14,15] Here, we were prompted to determine whether enhanced angiogenesis was also present in diabetic wounds treated with this system. We used von Willebrand Factor staining, one of the most widely used endothelial cell markers for studying angiogenesis. Blood vessel formation was compared between GAG-PA/K-PA and PBS treatment groups by the immunohistochemical staining with von Willebrand Factor and quantifications were performed based on its positive staining (Fig. 6A). As seen in Fig. 6B, the number of vessels per field was higher in the bioactive gel treated group compared to the control group on days 7 and 14. The number of blood vessels in GAG-PA/K-PA treated groups was also higher than control groups on day 21 but the difference was not statistically significant. This result revealed extensive neovascularization occurs in gel treated groups but not in control groups on days 7 and 14, suggesting that the peptide network is able to enhance wound healing by facilitating the formation of new blood vessels.

Furthermore, the angiogenic response of diabetic wounds was investigated through the western blot analysis of the VEGF protein level (Fig. 6C and D). The treatment of GAG-PA/K-PA significantly increased the VEGF levels on days 7 and 21. Interestingly, the administration of GAG-PA/K-PA on the wound site did not cause a significant difference on VEGF on day 14. VEGF level analyses further confirmed the presence of heightened angiogenic activity in diabetic wounds following heparin-mimetic PA treatment. The VEGF level was markedly elevated; around 3.5-fold higher in the bioactive gel treated group on day 7. This result is also consistent with the histological analysis of GAG-PA/K-PA treated wound tissue sections, which had a highly proliferative healing profile, especially on day 7.

3.5. α-SMA expression increases with bioactive gel treatment

The expression of α-SMA is a marker for the transition of fibroblast cells to myofibroblasts, which is essential for promoting wound contraction in tissue injury.[24] Besides myofibroblasts, α-SMA is expressed by pericytes, which are required for the maturation of blood vessels.[25] As such, α-SMA expression is an important marker for wound contraction and blood vessel maturation on wounds.

Immunohistochemical staining of wound tissue sections showed that the expression of α-SMA was higher in the bioactive gel treated group on day 14 compared to control (Fig. 7A and B). Furthermore, western blot analysis was performed for quantification of α-SMA expression in tissue samples, and confirmed our α-SMA immunohistochemical staining results (Fig. 7C and D). Similar to immunohistochemical analysis, protein levels of α-SMA increased two-fold following bioactive gel treatment compared to PBS control on day 14 (Fig. 7D).

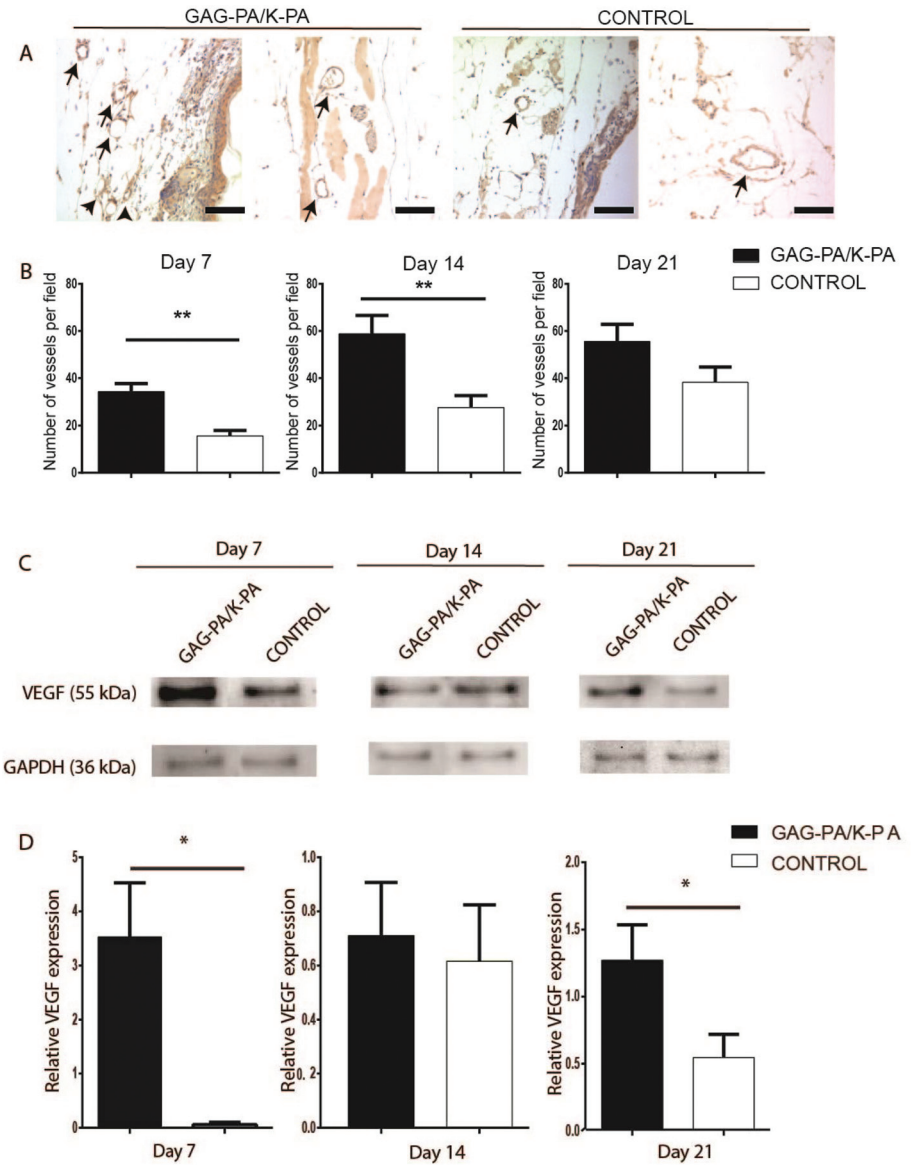

Fig. 6 Angiogenic response of diabetic wounds from GAG-PA/K-PA and PBS treated mice. Immunohistochemical staining for von Willebrand Factor (vWF) (A) and quantification based on vWF staining (B) of the wound areas showed that number of blood vessels in bioactive gel treatment was higher than control on days 7 and 14. Arrows indicate blood vessels (brown color) (A). Representative bands of GAG-PA/K-PA and control from western blot analysis of VEGF are shown in (C). VEGF level was quantified using western blot bands and normalized to GAPDH (D). Data are presented as means ± SEM, $*p < 0.05$, $**p < 0.01$.

However, α-SMA protein levels were very low and no change was observed between the groups at day 7, suggesting that the wounds were not mature enough to exhibit extensive α-SMA expression at this stage. On day 21, the wounds in all groups show increased expression of α-SMA, while a large (but statistically non-significant) difference was observed between the groups. Immunohistochemical staining for α-SMA also revealed extensive staining of blood vessel walls in the GAG-PA/K-PA treated wounds, suggesting that the VEGF level is upregulated in mice treated with the bioactive gel group. Increased α-SMA expression by myofibroblasts and pericytes enhanced wound contraction and granulation tissue maturation in the heparin-mimetic gel treated group on day 14. Myofibroblasts are largely responsible for wound contraction and produce extracellular matrix components such as type I and III collagens. The elevated α-SMA expression on day 14 is also correlated with ELISA results of the collagen I/III ratio in the bioactive gel treated group.

3.6. Heparin mimetic gel treatment affects wound inflammatory response

Characterization of an inflammatory response of db/db mice was performed by the ELISA analysis of two pro-inflammatory cytokines; IL-6 and TNF-α as shown in Fig. 8. IL-6 is a cytokine

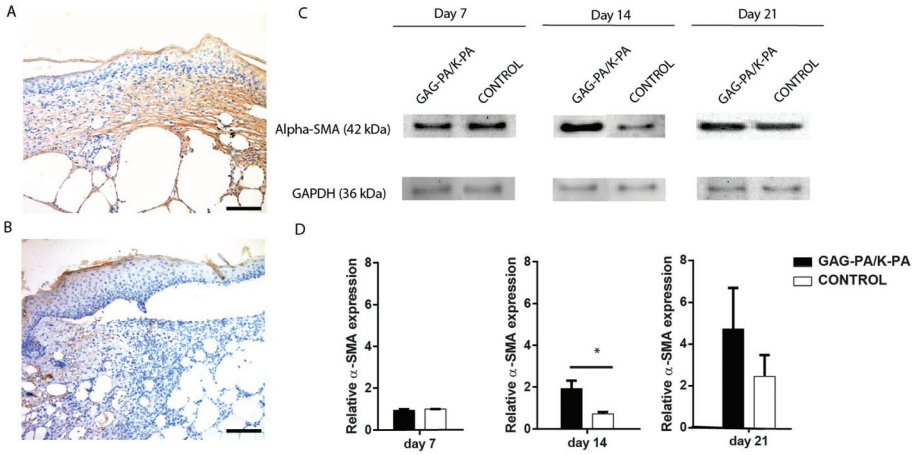

Fig. 7 α-SMA expression increased in the wound area of bioactive gel treated samples. Alpha-SMA staining (brown) of tissue sections treated with GAG-PA/KP-A (A) and PBS control (B) on day 14, with hematoxylin counterstaining of nuclei (blue). The quantification of α-SMA was based on western blot analysis and normalized to GAPDH (C, D). Significance levels were set at: $*p < 0.05$, scale bars = 200 μm.

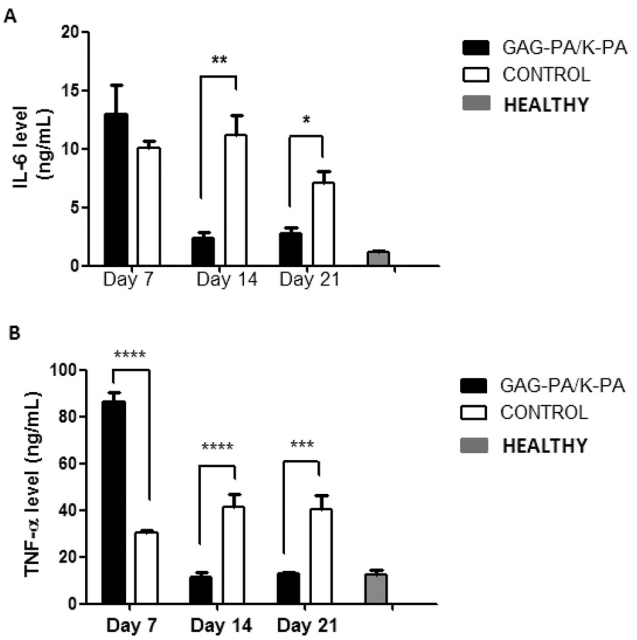

Fig. 8 Expression of the pro-inflammatory cytokines IL-6 (A) and TNF-α (B) in wound tissues on days 7, 14 and 21 and healthy (unwounded) controls. IL-6 and TNF-α levels were measured by ELISA. Significance levels were set at: $*p < 0.05$, $**p < 0.01$, $***p < 0.001$, $****p < 0.0001$.

that is strongly expressed in cutaneous wounds, and although it was not statistically significant, its expression in db/db wounds was found to increase following the application of heparin-mimetic PA gels to the wound site (on day 7). A significantly lower expression of the pro-inflammatory cytokine IL-6 was found in PA-treated wounds when compared with control at days 14 and 21 (Fig. 8A). There was a marked decrease of IL-6 expression in bioactive gel treated wounds compared to their PBS-control treated counterparts (4.5-fold on day 14 and 2.5-fold on day 21), suggesting that the inflammatory response is prolonged in PBS treated animals. Additionally, the expression level of IL-6 in bioactive gel treated animals was close to that of unwounded db/db mice at these time points. The expression of TNF-α was also found to exhibit a similar pattern as IL-6, with a significantly higher expression in both control and GAG-PA/K-PA-treated animals on day 7, which subsequently decreased on days 14 and 21 in the bioactive gel group but not in the PBS-treated group (Fig. 8B). These results suggest that treatment with GAG-PA/K-PA peptide nanofibers initially upregulates the expression of the pro-inflammatory cytokines IL-6 and TNF-α, but cytokine expression is then downregulated to mediate the transit from the inflammatory phase to the proliferative phase of wound healing.

While pro-inflammatory markers are strongly expressed in recently inflicted wounds and serve to recruit and activate macrophages and leukocytes at the site of injury,[26] their presence must gradually diminish for the healing process to continue. As such, a balance between pro-inflammatory and anti-inflammatory factors is necessary to stimulate the proliferation of native cells at the wound site following the initial recruitment of immune cells and the removal of cellular debris. In db/db mice; however, a strong IL-6 and TNF-α presence is observed at both early and later stages of wound healing, leading to the sustained presence of pro-inflammatory macrophages and the impairment of the recovery process.[27] Our ELISA analyses suggest that IL-6 and TNF-α expressions are high in both heparin-mimetic PA-treated and control groups at day 7, but rapidly decrease in the bioactive gel treated group by day 14 to a level comparable to unwounded skin. In contrast, immunoregulatory markers are still strongly present at the wound site at days 14 and 21 for the control group, suggesting that GAG-PA/K-PA (but not PBS) is able to modulate the immune response at the site of injury.

4. Conclusion

This study demonstrates that heparin-mimetic PA nanofibers were able to induce angiogenesis and accelerate wound healing in genetically diabetic db/db mice. The application of a bioactive gel to the wound site was found to accelerate wound closure, re-epithelialization, myofibroblast activation and blood vessel formation. It has been previously shown that heparin-mimetic PAs provide an environment that leads to the slow release of angiogenic growth factors, and especially VEGF. Molecular analysis of GAG-PA/K-PA treated wound tissues showed that the VEGF level was high even after 21 days following wounding. The remarkable increase in the VEGF level, together with positive α-SMA staining and extensive blood vessel formation at the wound site, suggests that angiogenesis is effectively induced by GAG-PA/K-PA in diabetic wounds. In addition, the expression of pro-inflammatory markers IL-6 and TNF-α initially increases and subsequently decreases in GAG-PA/K-PA treated rats. A marked decrease in the expression of both markers is a strong evidence of improved transition between the inflammatory and proliferative phases in heparin-mimetic gel treated animals. The results of this study indicate a potential use of heparin-mimetic peptide nanofibers for the treatment of diabetic wounds exhibiting impaired regeneration.

Acknowledgements

B. S and A. D. O were supported by TUBITAK BIDEB-2211C and 2211E PhD fellowships, respectively. S. T is supported by a TUBITAK BIDEB-2210E Master fellowship. This work is partially supported by TUBTIAK grant number 114S912. The authors thank Elif Arslan for SEM imaging, İbrahim Ulusoy for animal care and Zeynep Erdoğan for technical help.

References

1 B. C. Martin, J. H. Warram, A. S. Krolewski, R. N. Bergman, J. S. Soeldner and C. R. Kahn, *Lancet*, 1992, **340**, 925–929.
2 C. K. Sen, G. M. Gordillo, S. Roy, R. Kirsner, L. Lambert, T. K. Hunt, F. Gottrup, G. C. Gurtner and M. T. Longaker, *Wound Repair Regen.*, 2009, **17**, 763–771.
3 J. Boateng and O. Catanzano, *J. Pharm. Sci.*, 2015, **104**, 3653–3680.
4 D. Baltzis, I. Eleftheriadou and A. Veves, *Adv. Ther.*, 2014, **31**, 817–836.
5 H. Brem and M. Tomic-Canic, *J. Clin. Invest.*, 2007, **117**, 1219–1222.
6 K. E. Johnson and T. A. Wilgus, *Adv Wound Care*, 2014, **3**, 647–661.
7 M. Ladefoged, K. Buschard and A. M. Hansen, *APMIS*, 2013, **121**, 531–538.
8 M. Buck, K. Houglum and M. Chojkier, *Am. J. Pathol.*, 1996, **149**, 195–204.
9 J. M. Shah, E. Omar, D. R. Pai and S. Sood, *Indian J. Plast. Surg.*, 2012, **45**, 220–228.
10 R. M. Grossman, J. Krueger, D. Yourish, A. Granelli-Piperno, D. P. Murphy, L. T. May, T. S. Kupper, P. B. Sehgal and A. B. Gottlieb, *Proc. Natl. Acad. Sci. U. S. A.*, 1989, **86**, 6367–6371.
11 A. J. King, *Br. J. Pharmacol.*, 2012, **166**, 877–894.
12 M. C. Deeds, J. M. Anderson, A. S. Armstrong, D. A. Gastineau, H. J. Hiddinga, A. Jahangir, N. L. Eberhardt and Y. C. Kudva, *Lab. Anim.*, 2011, **45**, 131–140.
13 S. H. Bates, R. N. Kulkarni, M. Seifert and M. G. Myers, *Cell Metab.*, 2005, **1**, 169–178.
14 R. Mammadov, B. Mammadov, S. Toksoz, B. Aydin, R. Yagci, A. B. Tekinay and M. O. Guler, *Biomacromolecules*, 2011, **12**, 3508–3519.
15 R. Mammadov, B. Mammadov, M. O. Guler and A. B. Tekinay, *Biomacromolecules*, 2012, **13**, 3311–3319.
16 B. Senturk, S. Mercan, T. Delibasi, M. O. Guler and A. B. Tekinay, *ACS Biomater. Sci. Eng.*, 2016, **2**, 1180–1189.
17 R. Vasita and D. S. Katti, *Int. J. Nanomed.*, 2006, **1**, 15–30.
18 R. Nagaoka, K. Kobayashi and Y. Saijo, *Conf. Proc. IEEE Eng. Med. Biol. Soc.*, 2013, **2013**, 1112–1115.
19 S. McDougall, J. Dallon, J. Sherratt and P. Maini, *Philos. Trans. R. Soc., A*, 2006, **364**, 1385–1405.
20 L. Cuttle, M. Nataatmadja, J. F. Fraser, M. Kempf, R. M. Kimble and M. T. Hayes, *Wound Repair Regen.*, 2005, **13**, 198–204.
21 S. Velidandla, P. Gaikwad, K. K. Ealla, K. D. Bhorgonde, P. Hunsingi and A. Kumar, *J. Int. Oral Health*, 2014, **6**, 33–38.
22 J. Li, J. Chen and R. Kirsner, *Clin. Dermatol.*, 2007, **25**, 9–18.
23 A. J. Bailey, S. Bazin, T. J. Sims, M. Le Lous, C. Nicoletis and A. Delaunay, *Biochim. Biophys. Acta*, 1975, **405**, 412–421.
24 J. J. Tomasek, G. Gabbiani, B. Hinz, C. Chaponnier and R. A. Brown, *Nat. Rev. Mol. Cell Biol.*, 2002, **3**, 349–363.
25 Z. Ma, K. Shou, Z. Li, C. Jian, B. Qi and A. Yu, *Exp. Ther. Med.*, 2016, **11**, 1307–1317.
26 S. Guo and L. A. Dipietro, *J. Dent. Res.*, 2010, **89**, 219–229.
27 R. E. Mirza, M. M. Fang, W. J. Ennis and T. J. Koh, *Diabetes*, 2013, **62**, 2579–2587.